Selective Detection of H 2 Gas in Gas Mixtures Using NiO-Shelled Pd-Decorated ZnO Nanowires

Clémence Badie, Ali Mirzaei, Jae-hyoung Lee, Syreina Sayegh, Mikhael Bechelany, Lionel Santinacci, Hyoun Woo Kim, Sang Sub Kim

▶ **To cite this version:**

Clémence Badie, Ali Mirzaei, Jae-hyoung Lee, Syreina Sayegh, Mikhael Bechelany, et al.. Selective Detection of H 2 Gas in Gas Mixtures Using NiO-Shelled Pd-Decorated ZnO Nanowires. Advanced Materials Technologies, 2024, 10.1002/admt.202302081 . hal-04591002

HAL Id: hal-04591002
https://hal.science/hal-04591002v1

Submitted on 14 Oct 2024

HAL is a multi-disciplinary open access archive for the deposit and dissemination of scientific research documents, whether they are published or not. The documents may come from teaching and research institutions in France or abroad, or from public or private research centers.

L'archive ouverte pluridisciplinaire **HAL**, est destinée au dépôt et à la diffusion de documents scientifiques de niveau recherche, publiés ou non, émanant des établissements d'enseignement et de recherche français ou étrangers, des laboratoires publics ou privés.

Distributed under a Creative Commons Attribution 4.0 International License

Selective detection of H_2 gas in H_2/CO and H_2/NO_2 gas mixtures using NiO-shelled Pd-decorated ZnO nanowires as gas sensors

Clémence Badie,[1†] Ali Mirzaei,[2†] Jae-Hyoung Lee,[3] Syreina Sayegh,[4§] Mikhael Bechelany,[4,5#] Lionel Santinacci,[1§#] Hyoun Woo Kim,[6§#] and Sang Sub Kim[3§#]

[1]*Aix Marseille Univ, CNRS, CINaM, Marseille, France*

[2] *Department of Materials Science and Engineering, Shiraz University of Technology, Shiraz 715557-13876, Islamic Republic of Iran*

[3] *Department of Materials Science and Engineering, Inha University, Incheon 22212, Republic of Korea.*

[4]*Institut Européen des Membranes, IEM – UMR 5635, ENSCM, CNRS, University of Montpellier, Place Eugène Bataillon, 34095 Montpellier cedex 5, France.*

[5] *Gulf University for Science and Technology, GUST, Kuwait*

[6] *Division of Materials Science and Engineering, Hanyang University, Seoul 04763, Republic of Korea*

[†] *Co-first Authors*

[§] *Co-last authors*

[#] *Corresponding authors*

Abstract
Hydrogen (H_2) gas is a green fuel, but its leakage during storage and transportation can lead to disasters due to its explosive nature. Here, we developed a sensitive and selective H_2 gas sensor that can detect H_2 in H_2/CO and H_2/NO_2 gas mixtures. First, ZnO nanowires (NWs) were grown using vapor-liquid-solid (VLS) growth. This was followed by atomic layer deposition (ALD)-mediated growth of Pd nanoparticles (NPs) on the ZnO NWs and uniform deposition of a thin NiO shell layer (12 nm in thickness) over the Pd-decorated ZnO NWs. Characterization of the synthesized samples by different methods confirmed the desired chemical composition, morphology and phases. H_2 gas sensing studies revealed the highly sensitive and selective response of the optimized gas sensor to H_2 at 200°C. In the presence of H_2/CO and H_2/NO_2 gas mixtures, the NiO-shelled Pd-decorated ZnO NW, but not the Pd-decorated ZnO NW gas sensor displayed good selectivity for H_2. Furthermore, the NiO-shelled Pd-decorated ZnO NW gas sensor efficiently detected H_2 even in the presence of 40% relative humidity and displayed good stability even after one month. The present results can open the doors towards the fabrication of highly selective H_2 gas sensors using the described rationale design.

Keywords: ZnO nanowire; NiO shell; Pd decoration; ALD; H_2 gas sensor; Selectivity; Sensing mechanism.

1. Introduction

Hydrogen (H_2) gas is considered a next-generation green fuel: it is renewable, releases a significant amount of heat during combustion, and does not produce toxic emissions. Currently, H_2 gas is used in hydrogen fuel cells for electric vehicles and its reducing capacities are exploited in metal reduction, chemical industry, and petroleum extraction. However, H_2 has some safety issues. At concentrations between 4 and 75 vol% it is an explosive gas characterized by low ignition energy (0.02 mJ) and large flame propagation velocity. Moreover, it can easily leak due to its small molecule size (θ_k = 0.29 nm) and high diffusion coefficient in air (0.6 cm^2/s), which may cause sudden explosions. In addition, it can cause asphyxia by replacing O_2 in air. As H_2 gas is without color, odor and taste, H_2 gas sensors are needed to detect leaks [1]. H_2 gas is also used in clinical settings for the treatment of asthma and chronic obstructive pulmonary disease. Moreover, it reduces neuronal cell apoptosis and promotes tumor cell apoptosis [2].

Chemiresistive gas sensors with metal oxides are particularly interesting due to their high response, high stability, fast dynamics, ease of fabrication and operation, and low price. However, metal oxide gas sensors operate at high temperatures (150–450°C) and often display poor selectivity [3].

In general, the sensing performance of n-type (e.g. SnO_2 and ZnO) gas sensors is better than that of p-type metal oxide gas sensors, mostly linked to their high electron mobility [4]. Among n-type metal oxides, ZnO is a promising sensor material due to its stability, high electron mobility, desirable band gap (E_g = 3.6 eV), ease of synthesis, availability and low price. However, like other metal oxide gas sensors, it exhibits poor selectivity in the pristine form because it shows similar responses to most gases [5]. Various approaches have been investigated to improve the selectivity of ZnO and other metal oxide gas sensors: metal doping [6], noble metal decoration [7], n-n heterojunction formation [8], n-p heterojunction formation [9] and use of filters [10].

Noble metal decoration can increase the sensing performance, especially in term of selectivity, through two mechanisms. The first is related to the catalytic effect of noble metals, in which the incoming gas molecules become easily adsorbed on the noble metal and are then dissociated to smaller ions that can move to the surface of neighboring metal oxide. For example, it is well-accepted that Pd nanoparticles (NPs) can dissociate H_2 molecules to atomic H and increase their reactions with adsorbed oxygen ions [11]. The second mechanism is related to the formation of heterojunctions between noble metals and metal oxides, leading to extensive resistance modulation [12]. In this study, we used Pd to decorate ZnO nanowires (NWs) due to its good catalytic activity towards H_2 gas [1a, 1d, 13].

However, decoration of metal oxide surfaces with of noble metals can lead to poisoning in the presence of some gases. For instance, Pd poisons include many organic and inorganic chemicals that contain sulfur (H_2S, SO_2, thiols) and phosphorous [1d, 14]. This may affect their catalytic activity and limit metal NP role as promising agents to enhance gas sensing performance. Furthermore, as gas sensors operate at high temperatures, ultrathin noble metals might be oxidized in air, decreasing the sensing performance, and noble metals might agglomerate on the sensor surface [15]. Therefore, it is essential to find a way to protect the noble metals from direct exposure to air in order to enhance the sensing properties. The deposition of a thin metal oxide layer over the decorated NPs could be a promising protective strategy, which has been less studied for ternary systems. In this study, we used NiO as deposition layer over the Pd-decorated ZnO NWs. In addition, to prevent Pd poisoning, p-type NiO is interesting because it displays very good structural stability, good oxygen adsorption, and strong catalytic activity [4]. In the absence of Pd decoration of the ZnO surface, NiO is in direct contact with ZnO. Intimate contacts between n-ZnO and p-NiO can provide numerous heterojunctions with potential barriers to flow of charges in air. Upon exposure to the target gas, the barrier height changes, leading to resistance modulation of the sensor [16]. Previous studies described enhanced performance of ZnO-NiO heterojunctions for gas sensing applications compared with their pristine counterparts [17]. Moreover, as NiO is deposited as a continuous layer, a core-shell structure is expected where ZnO and NiO are in direct contact. This should maximize the contact area between components, leading to significant resistance modulation [18]. On the other hand, when Pd NPs are placed between two layers of ZnO and NiO, ZnO-Pd-NiO heterojunctions are formed [19]. Modulation of the barriers formed between these materials can strongly influence the sensing mechanism.

Atomic layer deposition (ALD) is a reliable deposition technique and it is perfectly suitable for coating core materials with conformal and uniform thin layers [20]. ALD allows controlling the Pd NP thickness at the sub-nanometer scale and also their relatively narrow size distribution [21]. NiO and Pd have already been grown by ALD [22]. Pd/Ni catalysts deposited on nanoporous Al_2O_3 display good activity in formic acid electrooxidation [23]. Moreover, Pd deposition on Ni/NiO nanofibers shows electrochemical hydrogen and oxygen evolution reactions [24]. More recently, NiO layer deposition on porous In_2O_3 has been used to boost NO_2 detection [25].

On the basis of these findings, here, first ZnO NWs were easily synthesized by vapor-liquid-solid (VLS) growth as previously described [26]. Then, Pd NPs were decorated over the synthesized ZnO NWs using ALD. This was followed by deposition of a NiO shell (12 nm in thickness) over the Pd-decorated ZnO NWs.

As expected, this work demonstrated the beneficial effect of Pd NPs on the ZnO NW sensitivity. Although the NiO shell weakened the raw response of the device, it significantly increased its selectivity when H_2 was mixed with CO and NO_2. These properties demonstrate the interest of such gas sensor architecture for use in realistic conditions.

2. Experimental

2.1. Growth of ZnO NWs

Networked ZnO NWs were directly grown on a patterned electrode substrate using VLS growth with an Au-catalyst as previously described [26-27]. Briefly, tri-layered interdigital electrodes (TIEs) were sputter-deposited on SiO_2 (200 nm thick)-covered Si (100) substrates with the following sequence: Ti (50 nm), Pt (200 nm), and Au (3 nm). Then, the substrate with TIEs was placed into a quartz tube furnace at a fixed distance from a ceramic boat containing metallic Zn powder (99.9%) placed at the furnace center. The temperature increase to 900 °C, in an atmosphere containing flowing N_2 (300 sccm) and O_2 (10 sccm) gases, led to the melting of the Au catalyst and to the generation of Zn vapors that were moved towards the substrate by the carrier gas (N_2). Zn diffused into the Au droplets and ZnO directional growth at the substrate/droplets interface began when the droplets became supersaturated with Zn atoms. The networked ZnO NWs were grown on the TIE for 30 min and they became entangled in the areas between the electrodes.

2.2. Pd NP deposition by ALD

Pd NPs were deposited on ZnO NWs in a home-built ALD reactor [28)]at 220°C using $Pd(hfac)_2$ (95% from Strem Chemicals) heated to 70°C and formalin (37% formaldehyde in water with 10-15% methanol; Sigma-Aldrich) as precursor and co-reactant, respectively, as described earlier [29]. Each ALD cycle was as follows: Pd pulse for 5 s, exposure for 15 s and Ar purge for 10 s, followed by CH_2O pulse for 1 s, exposure for 15 s and Ar purge for 60 s. N_{Pd} = 100 cycles were used to obtain the desired Pd NPs.

2.3. NiO layer deposition by ALD

NiO was deposited on Pd-decorated ZnO NWs and on Si (100). For deposition on Si, the wafers were cut into 1×1 cm^2 pieces and were degreased by sonication in acetone, isopropanol, methanol and ultra-pure water, followed by dipping in 5% hydrofluoric acid solution for 30 s. After abundant rinsing in ultra-pure water and drying under a nitrogen stream, NiO films were grown by thermal ALD in a showerhead geometry reactor Fiji 200 (Veeco/Cambridge Nanotech), as previously described [30]. $Ni(CpEt)_2$ (99.99%, Strem Chemicals) and O_3 generated from O_2 were used as Ni precursor and O source, respectively. Ar (≥ 99.999%, from Linde Electronics) served as vector gas. $Ni(CpEt)_2$ was maintained at 94°C and the chamber temperature was fixed at T_{NiO} = 250°C. ALD sequence consisted of pulsing and purging successively $Ni(CpEt)_2$ and O_3 for defined times with an additional exposure step after each pulse to uniformly cover the ZnO NWs. The ALD sequence (pulse/exposure/purge) was set as follows for $Ni(CpEt)_2$ and O_3: 2/15/34 s and 0.3/12/34 s, respectively. The films thickness (t_{NiO}) was modulated by choosing the number of ALD cycles (N_{NiO}) according to the earlier defined growth per cycle of 0.2 Å/cycle[30].

2.4. Characterization

Morphology was investigated by scanning and transmission electron microscopy (SEM and TEM), using JSM 7900F (JEOL Ltd) and JEM 2010 (JEOL Ltd), respectively. The crystal structure was studied by selected-area electron diffraction (SAED) performed with TEM. The different elements were localized by energy-dispersive X-ray spectroscopy (EDS) (Quantax FlatQuad, Bruker). The chemical composition was assessed by X-ray photoelectron spectroscopy (XPS; Kratos Analytical, UK) with a monochromatic Al K_α source (1486.6 eV). The binding energy (BE) was corrected using the C 1s peak at 284.8 eV. Curves were fitted with CASAXPS, version 2.3.25, a Shirley background subtraction routine and

Lorentzian/Gaussian components. NiO thickness was measured in situ with a M2000V spectroscopic ellipsometer (J. A. Woollam Inc).

2.5. Gas sensing measurements

The method used for gas sensing measurements was previously described [31]. The gas sensors under study were exposed to different gases at various temperatures using a homemade sensing system. The target gas concentration was monitored by adjusting the target gas-to-dry air ratio using accurate mass flow controller devices (total flow rate = 500 sccm). During measurements, the gas sensor resistance changes in air (R_a) and in the presence of the target gas (R_g) were automatically recorded. The response was defined as $R = R_a/R_g$. The sensor response time was defined as the time needed to reach 90% of the final resistance after exposure to the target gas and the recovery time was the time needed to recover 90% of the initial resistance after removal of the gas.

3. Results and discussion

3.1. Morphological and chemical studies

Figure 1a shows the ZnO NWs grown over the TIE substrate and **Figure 1b** a SEM image of ZnO NWs. As ZnO NW size depends on the initial size of the as-formed Au-droplets, ZnO NWs with different sizes, but with a narrow size distribution, were synthesized. The diameter of a ZnO NW was >70 nm (**Fig. 1c**). **Figure 1d** shows a single ZnO NW uniformly covered by a dense film of Pd NPs after Pd deposition by ALD.

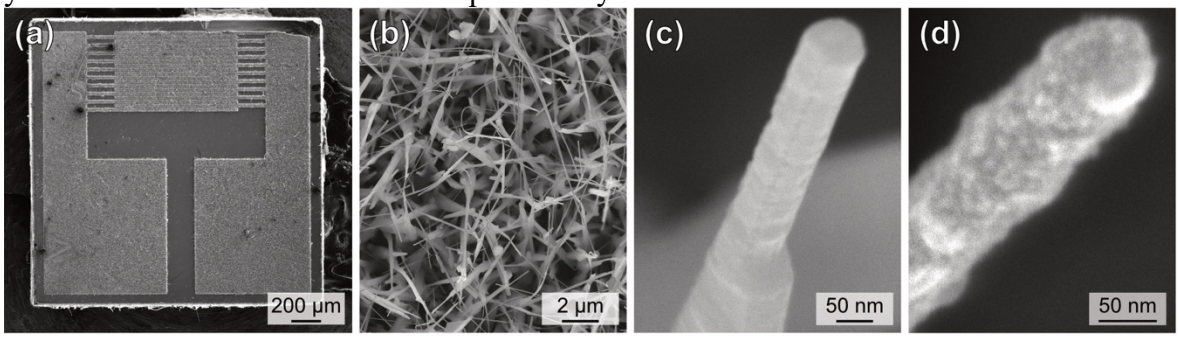

Fig. 1. SEM images of (a) VLS-grown ZnO NWs on the substrate, (b) ZnO NW network, (c) a single ZnO NW, and (d) a single ZnO NW coated by Pd NPs.

High-resolution TEM (**Fig. 2a**) showed that bare ZnO NWs had a crystalline structure, with spacings between the parallel fringes of 0.519 and 0.273 nm, attributed to the {0001} and {01-10} ZnO planes, respectively. TEM analysis of the NiO shell over a Pd-decorated ZnO NW (**Fig. 2b**) showed a uniform coating by the NiO shell thanks to ALD deposition. The spotty SAED pattern of bare ZnO (**Fig. 2c**) showed the single crystalline nature of bare ZnO NWs. In the SAED pattern of Ni-shelled Pd-decorated ZnO NWs (**Fig. 2d**), the spotty pattern related to ZnO and the ring patterns related to NiO and Pd with a polycrystalline nature could be seen. The weak intensity of the circles may be explained by the layer thin thickness or the presence of small imbedded crystallites. The white circles corresponded to Pd NP diffraction. A thorough analysis revealed that the circles were composed of small spots coming from each monocrystalline NP. TEM images of ZnO NWs after deposition of Pd and NiO (**Fig. 2e-f**) showed that the NiO shell completely covered the Pd-decorated ZnO NWs which had a diameter from 60 to 120 nm. In addition, Moiré fringes (white arrows in **Fig. 2f**) demonstrated the superposition of lattice planes.

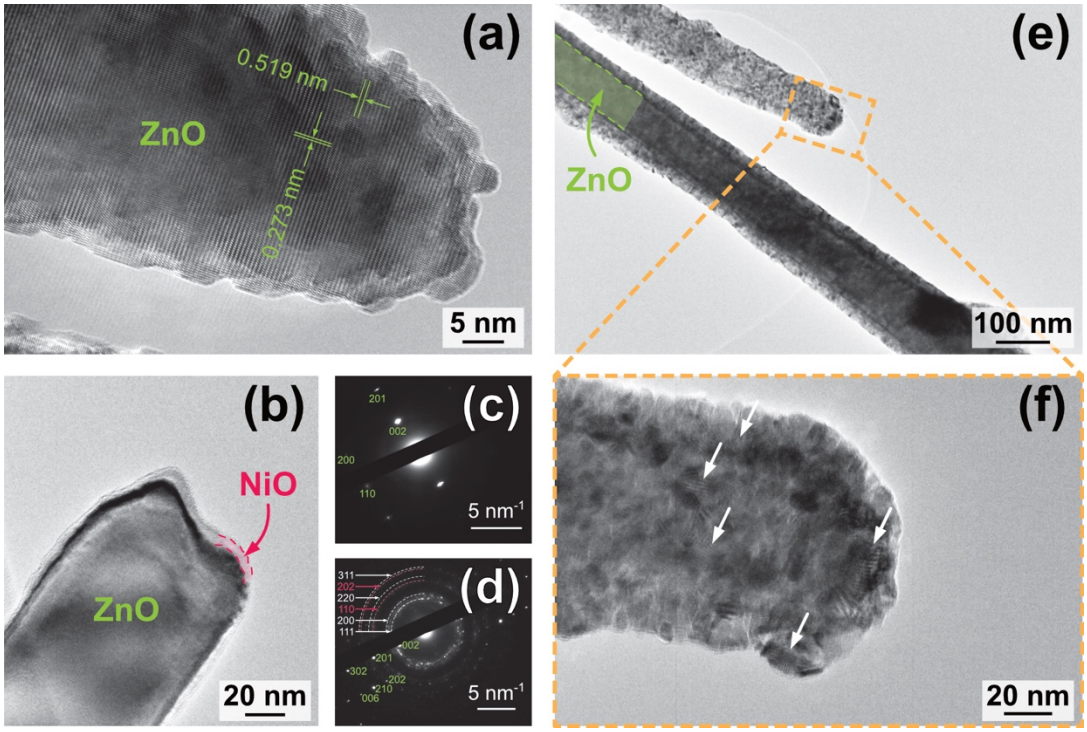

Figure 2. Representative TEM photographs of (a) a bare single ZnO NW and (b) a NiO-shelled Pd-decorated ZnO NW. SAED patterns of a (c) bare and (d) Ni-shelled Pd-decorated ZnO NW. (e) Low and (f) high magnification TEM photographs of NiO-shelled Pd-decorated ZnO NWs. The box in (e) corresponds to the high-magnification area in (f).

EDS chemical analysis of a single NiO shelled Pd-decorated ZnO NW during the SEM (**Fig. 3a**) showed the presence of the peaks related to Zn, Ni, Pd and O in addition to those related to the Si substrate and the usual carbon contamination (**Fig. 3b**). EDS mapping confirmed the presence of Zn, Ni and Pd elements (**Figs. 3c-3e**). Oxygen mapping is not shown because oxygen was detected on the entire scrutinized area. Zn and Ni were uniformly distributed, confirming the full coverage of the ZnO NW by the NiO shell. Distinct Pd NPs could not be observed in **Figure 3e** due to the high particle density and because the Pd signal had to pass through the NiO film.

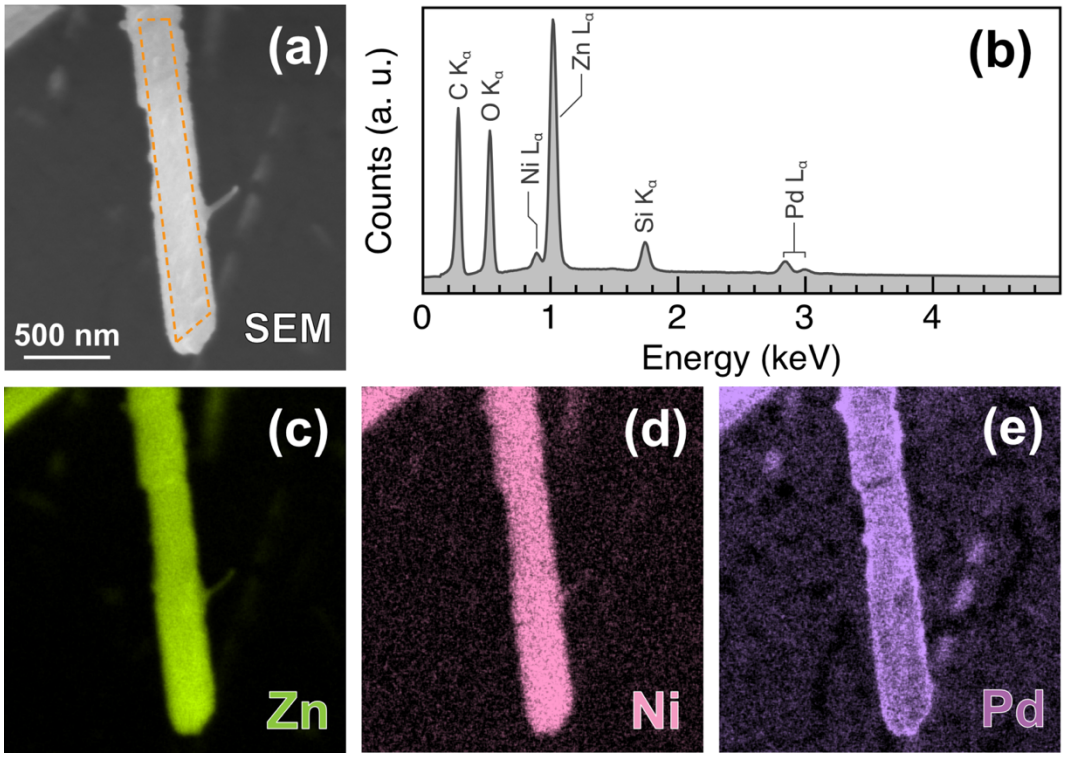

Fig. 3. EDS spectrum and mapping of a single sensing NW. (a) SEM image of a typical NiO-shelled Pd-decorated ZnO NW. (b) EDS spectrum corresponding to the boxed area in (a). EDS mapping of (c) Zn (d) Ni and (e) Pd in the NiO shelled Pd-decorated ZnO NW.

The chemical states of NiO-shelled Pd-decorated ZnO NWs were analyzed by XPS (**Fig. 4**). XPS peaks and some Auger electron transitions of the constituting elements (Zn, Ni, Pd, O) were detected on the survey spectrum (**Fig. 4a**) as well the peaks related to Si (substrate) and C (adventitious carbon). The Zn 2p spectrum (**Fig. 4b**) included a single contribution (Zn–O), with a BE of 1022.1 eV (Zn $2p_{3/2}$) and a spin-orbit-splitting (SOS) of 23.2 eV. This corresponds to ZnO in the literature [32]. **Figure 4c** shows Ni $2p_{3/2}$ contribution and its satellite peaks. For clarity, the $2p_{1/2}$ area is not shown, but its position relative to $2p_{3/2}$ corresponded to the expected SOS for NiO (18.4 eV) [32a]. As previously reported [33], the $2p_{3/2}$ peak was fitted with two contributions (BE = 854.1 and 855.9 eV), both assigned to NiO and hydroxylated Ni (the latter located mainly at the surface). Additional contributions were measured at BE = 861.0 and 863.5 eV, and were attributed to the satellite peaks. The Pd $3d_{5/2}$ and $3d_{3/2}$ peaks (**Fig. 4d**) had the expected SOS = 5.2 eV [32a, 34]. The Pd $3d_{5/2}$ and $3d_{3/2}$ peaks exhibited two contributions: i) BE = 335.2 for Pd $3d_{5/2}$ and BE = 340.4 eV for $3d_{1/2}$ (low energy contribution), assigned to metallic palladium (Pd^0) and ii) BE = 336.6 for Pd $3d_{5/2}$ and BE = 341.8 eV for $3d_{1/2}$ (high energy contribution), attributed to Pd^{2+}[34-35] and corresponding to Pd bonded to the O of NiO. The O 1s peak (**Fig. 4e**) also included two contributions: i) BE = 529.6 eV ascribed to O^{-II} bonded to a metal, such as Ni [30, 36]. However, as Zn was detected, a small contribution can also arise from oxygen bonded to Zn from the ZnO NWs underneath the NiO layer [37]; and ii) BE = xy that displayed the largest intensity. It was attributed to several contributions, particularly O bonded to Ni^{II} [30, 36] and Pd^{II} [34]. This component was also related to superficial contamination [38], such as hydroxyl groups. Lastly, the C 1s region (**Fig. 4f**) corresponded to adventitious carbon impurities and presented three contributions corresponding to C–C (BE = 284.8 eV), C–O (BE = 286 eV), and C=O (BE = 288.5 eV) [38-39].

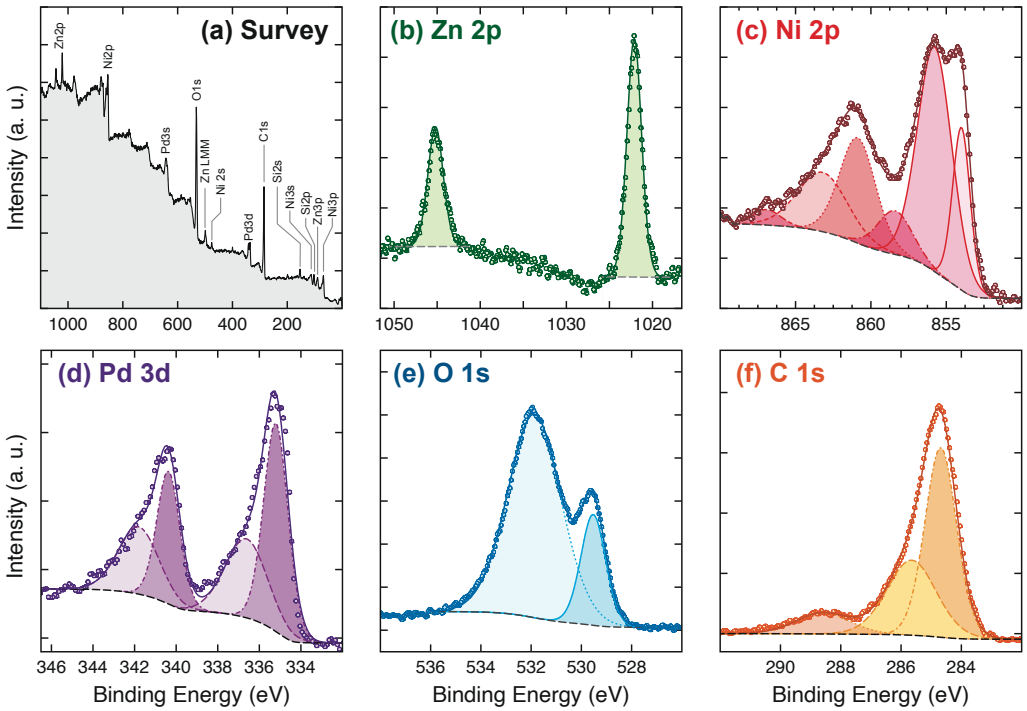

Fig. 4. XPS analysis of NiO-shelled Pd-decorated ZnO NW. (a) Survey spectrum, (b) Zn 2p (c), Ni 2p, (d) Pd 3d and (e) O 1s spectra, and (f) C 1s core-level regions.

3.2. Gas sensing studies

First, the fabricated gas sensors (ZnO NWs, Pd-decorated ZnO NWs, and NiO-shelled Pd-decorated ZnO NWs) were exposed to various concentrations of H_2 gas (1, 10, 100 and 500 ppm) at different temperatures in order to identify their optimal sensing temperature. The dynamic resistance curves (**Fig. 5a-c**) showed that all sensors had an n-type behavior, in which their resistances decreased upon injection of H_2 gas with a reducing nature. This indicates that the behavior of these sensors is mostly governed by ZnO (n-type behavior). Moreover, the gas sensor responses were strongly influenced by the temperature (**Fig. 5d-f**). Specifically, with the pristine ZnO NW gas sensor, no sensing signal was detected at 25 and 50°C. At 100°C, it showed a very low response to 100 ppm and 500 ppm H_2 gas. The response gradually increased with the increasing temperatures and the maximum response was observed at 250°C. However, this response was not high (e.g. 6.1 to 500 ppm H_2 gas at 250°C). Conversely, the Pd-decorated ZnO NW sensor showed a low response to H_2 gas even at room temperature. Its response progressively increased up to 200°C (41.01 to 500 ppm H_2 gas) and was strongly decreased at 250°C. The NiO-shelled Pd-decorated ZnO NW gas sensor showed a similar response profile: the response increased up to 200°C (16.12 to 500 ppm H_2 gas) and then decreased. The low response at low temperatures was due to the fact that there was not enough energy for H_2 to overcome the adsorption barrier. With temperatures above the optimal temperature, the desorption rate was higher than the adsorption rate and the gas response decreased again. At the optimal temperature, the adsorption was maximum and the highest response to H_2 gas was observed. Based on the above findings, the optimal sensing temperature was 200°C for Pd-decorated ZnO NWs and NiO-shelled Pd-decorated ZnO NWs and the other tests were performed at this temperature. Due to the low response of the pristine ZnO NW gas sensor, it was not used for the next experiments.

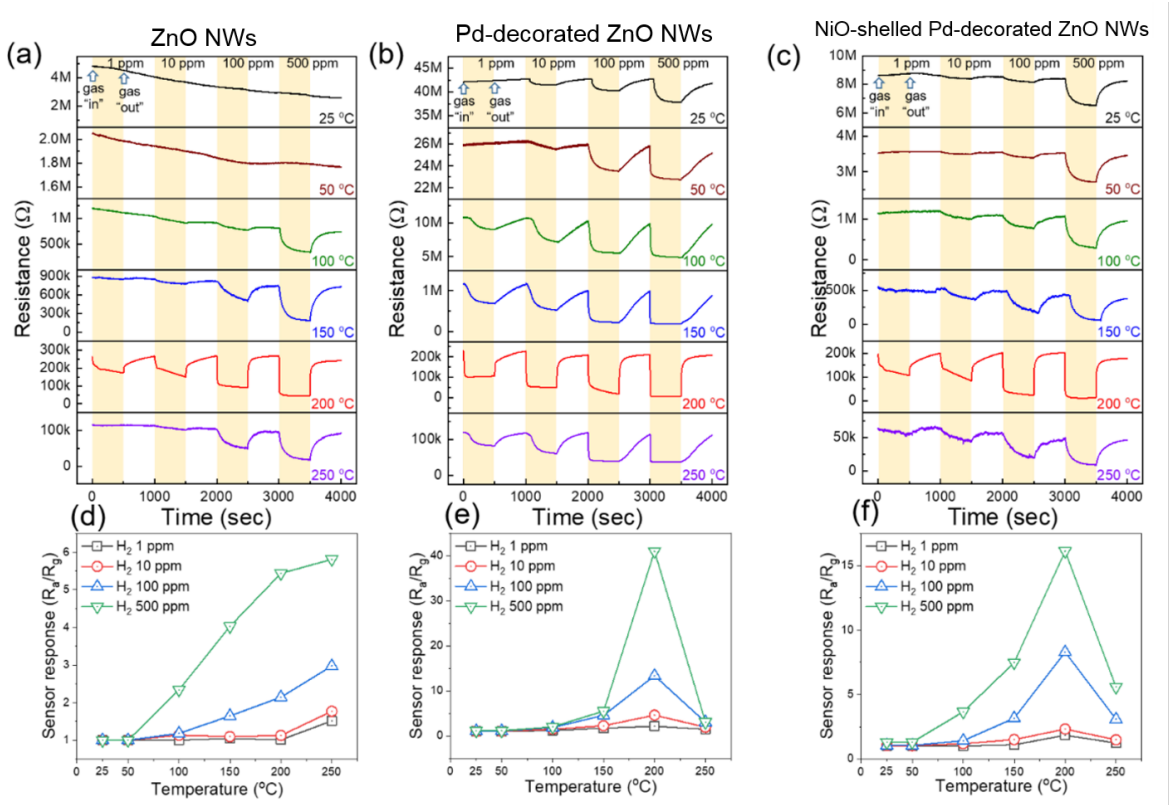

Fig. 5. (a) Dynamic resistance curves of (a) pristine ZnO NWs, (b) Pd-decorated ZnO NWs, and (c) NiO-shelled Pd-decorated ZnO NW gas sensors in the presence of 1, 10, 100 and 500 ppm H_2 gas at the indicated temperatures. Sensor response in function of the temperature for (d) pristine ZnO NWs, (e) Pd-decorated ZnO NWs, and (f) NiO-shelled Pd-decorated ZnO NW gas sensors at different H_2 gas concentrations.

In the next step, the selectivity for H_2 of Pd-decorated ZnO NW and NiO-shelled Pd-decorated ZnO NW gas sensors was studied by calculating the dynamic resistance curves in the presence of increasing concentrations of H_2 gas (1, 10, 100 and 500 ppm H_2 gas) alone or mixed with 500 ppm CO gas or NO_2 gas at 200°C. Upon exposure of Pd-decorated ZnO NWs to pure H_2, which is a reducing atmosphere, resistance decreased (**Fig. 6a**). This demonstrated the n-type behavior of the sensor. Indeed, ZnO is an n-type metal oxide semiconductor due to the presence of oxygen vacancies. The response values were 2.14 (1 ppm H_2 gas), 4.61 (10 pm H_2 gas), 13.36 (100 ppm H_2 gas) and 41.01 (500 ppm H_2 gas). When H_2 gas at different concentrations was mixed with 500 ppm CO gas, the response values were 1.08, 1.17, 2.57 and 12.11 for 1, 10, 100 and 500 ppm H_2 gas, respectively. When H_2 gas at different concentrations (1, 10, 100 and 500 ppm) was mixed with 500 ppm NO_2 gas, the response values were 1, 1.05, 1.75 and 6.39, respectively. These data highlighted the significant response decrease in the presence of CO and NO_2 gases. When NiO-shelled Pd-decorated ZnO NWs were tested in the same conditions (**Fig. 6b**), the sensor resistance decreased upon exposure to H_2 alone, indicating again the sensor n-type behavior. It also revealed that the sensing behavior was governed by ZnO n-type behavior, despite the presence of NiO, a p-type semiconductor. The response values were 1.84 (1 ppm H_2 gas), 2.32 (10 ppm H_2 gas), 8.29 (100 ppm H_2 gas), and 16.12 (500 ppm H_2 gas). When 1, 10, 100 and 500 ppm H_2 gas were mixed with 500 ppm CO gas and with 500 ppm NO_2 gas, the response values were 1.15, 1.31, 2.6 and 12.41 and 1.19, 1.39, 2.95 and 13.19, respectively. NO_2 is an oxidizing compound that leads to the increase of n-type gas sensor resistance. However, with both Pd-decorated ZnO NWs and NiO-shelled Pd-decorated

ZnO NWs, the sensor resistance decreased also when exposed to H_2 mixed with NO_2 gas. This indicated that the sensors are more sensitive to H_2 than NO_2.

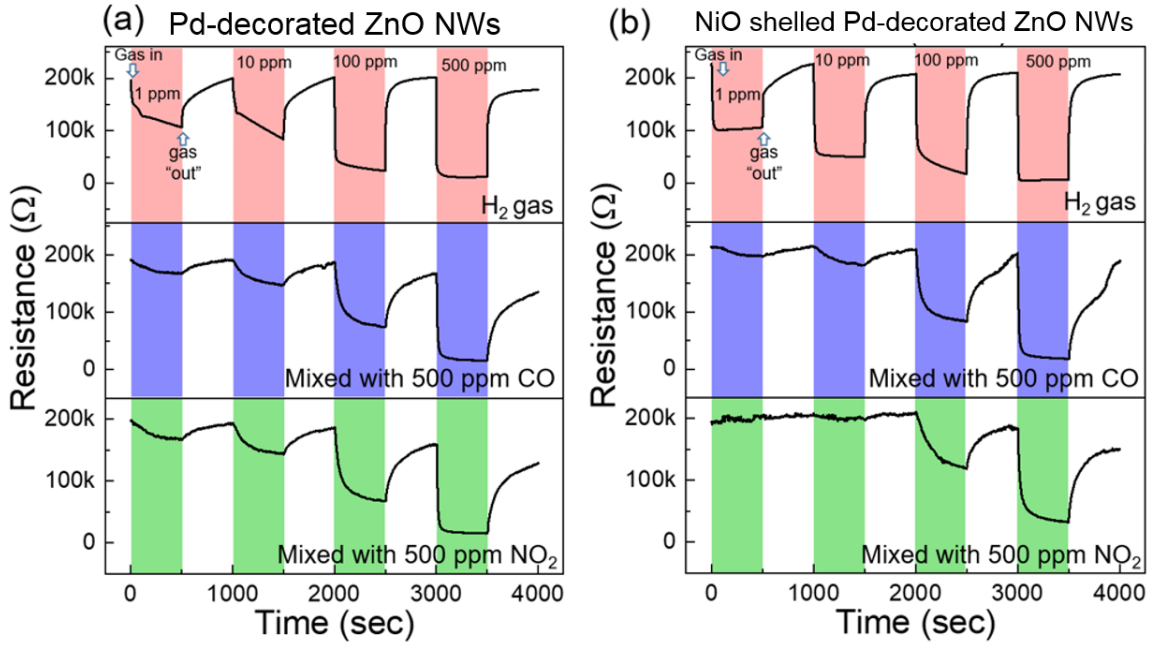

Fig. 6. Dynamic resistance curves of (a) Pd-decorated ZnO NW and (b) NiO-shelled Pd-decorated ZnO NW gas sensors to 1, 10, 100 and 500 ppm H_2 gas and to mixtures of different concentrations of H_2 and 500 ppm CO or 500 ppm NO_2 at 200°C.

To better understand the sensing behavior of the two sensors towards the target gases, their response to pure H_2 gas and mixed with 500 ppm CO or 500 ppm NO_2 gases was compared. Overall, the response of the Pd-decorated ZnO NW sensor (**Fig. 7a**) significantly decreased upon exposure to the gas mixtures. For example, the response values were 41.01 to 500 ppm pure H_2 and 12.11 and 6.39 to 500 ppm H_2 + 500 ppm CO and 500 ppm H_2 + 500 ppm NO_2 gases. Conversely, the response of NiO-shelled Pd-decorated ZnO NWs did not significantly change when exposed to gas mixtures (**Fig. 7b**). Indeed, the response values were 16.12 (500 ppm H_2 gas), 12.41 (500 ppm H_2 + 500 ppm CO) and 13.19 (500 ppm H_2 + 500 ppm NO_2), respectively. Then, comparison of the responses of Pd-decorated ZnO NW and NiO shelled Pd-decorated ZnO NW gas sensors to various concentrations of H_2 mixed with 500 ppm NO_2 at 200°C (**Fig. 7c**) showed that the response of NiO shelled Pd-decorated ZnO NWs was always higher than that of Pd-decorated ZnO NWs. For example, the response values of NiO-shelled Pd-decorated ZnO NWs and Pd-decorated ZnO NWs to 500 ppm H_2 and 500 ppm NO_2 were 13.19 and 6.39. A similar trend was observed for all H_2 concentrations in the presence of 500 ppm CO (**Fig. 7d**). For example, the response values of NiO-shelled Pd-decorated ZnO NWs and Pd-decorated ZnO NWs to the 500 ppm H_2 + 500 ppm CO mixture were 12.41 and 12.11, respectively. This showed again the superiority of the NiO-shelled Pd-decorated ZnO NW system compared with Pd-decorated ZnO NWs because it displayed similar responses to pure H_2 and to H_2 mixed with CO and NO_2 gases.

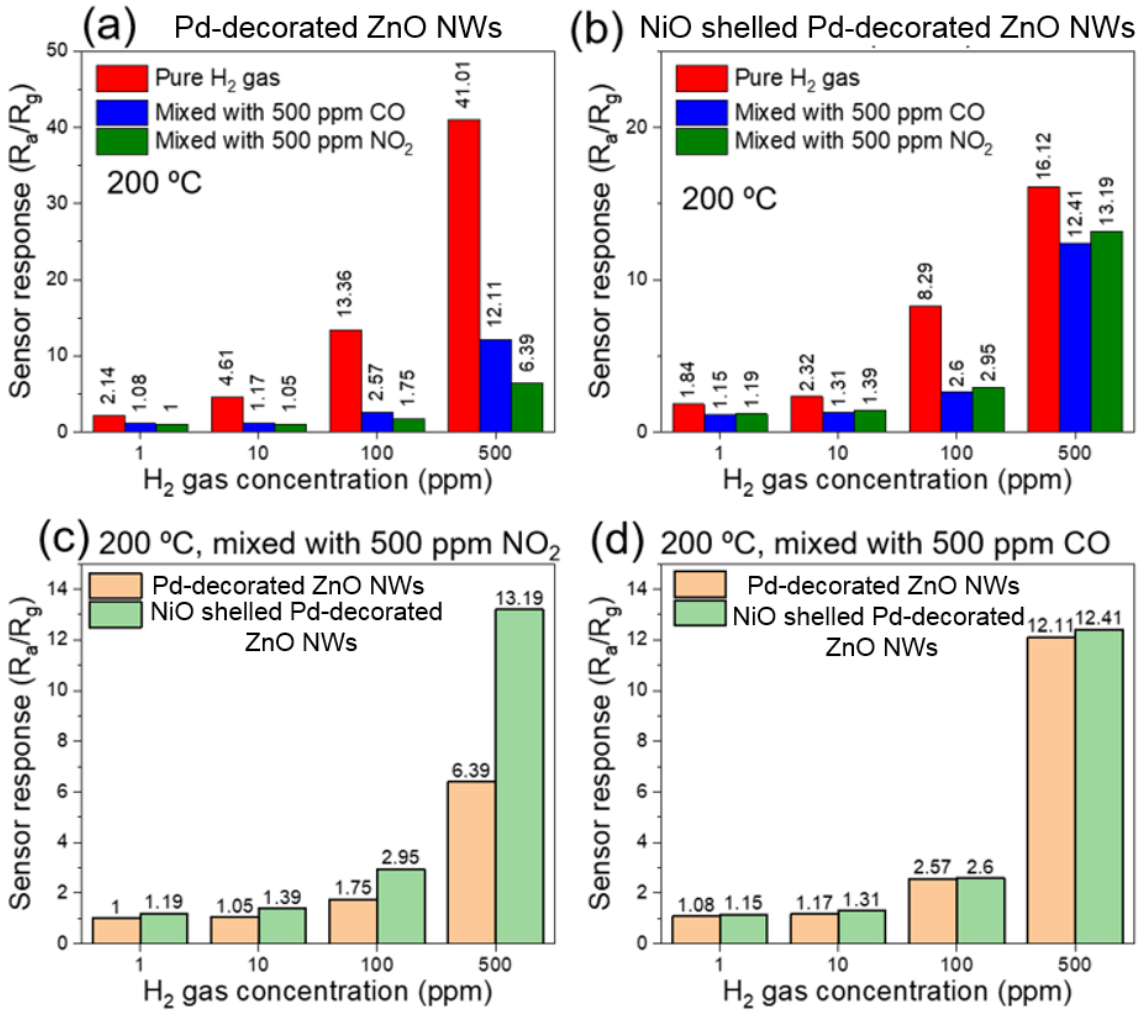

Fig. 7. Responses of (a) Pd-decorated ZnO NW and (b) NiO-shelled Pd-decorated ZnO NW sensors to 1, 10, 100, and 500 ppm H_2 gas and to H_2 (different concentrations) mixed with 500 ppm CO or 500 ppm NO_2 at 200°C. Comparison of the responses of Pd-decorated ZnO NWs and NiO-shelled Pd-decorated ZnO NWs to H_2 (different concentrations) mixed with (c) 500 ppm NO_2 gas and (d) 500 ppm CO gas at 200°C.

To assess repeatability, the two gas sensors were used for five sequential cycles (100 ppm H_2 and mixtures of 100 ppm H_2 with 500 ppm CO or 500 ppm NO_2 gas at 200°C). The resistance values of the two sensors did not significantly change during the five gas sensing cycles (**Fig. 8a and c**). To precisely monitor the sensing behaviors, the responses of Pd-decorated ZnO NWs and NiO-shelled Pd-decorated ZnO NWs were calculated in function of the cycle number (**Fig. 8b and d**). The Pd-decorated sensor response slightly fluctuated during the five cycles. Conversely, the NiO-shelled Pd-decorated ZnO NW response remained almost constant during the five sequential sensing cycles.

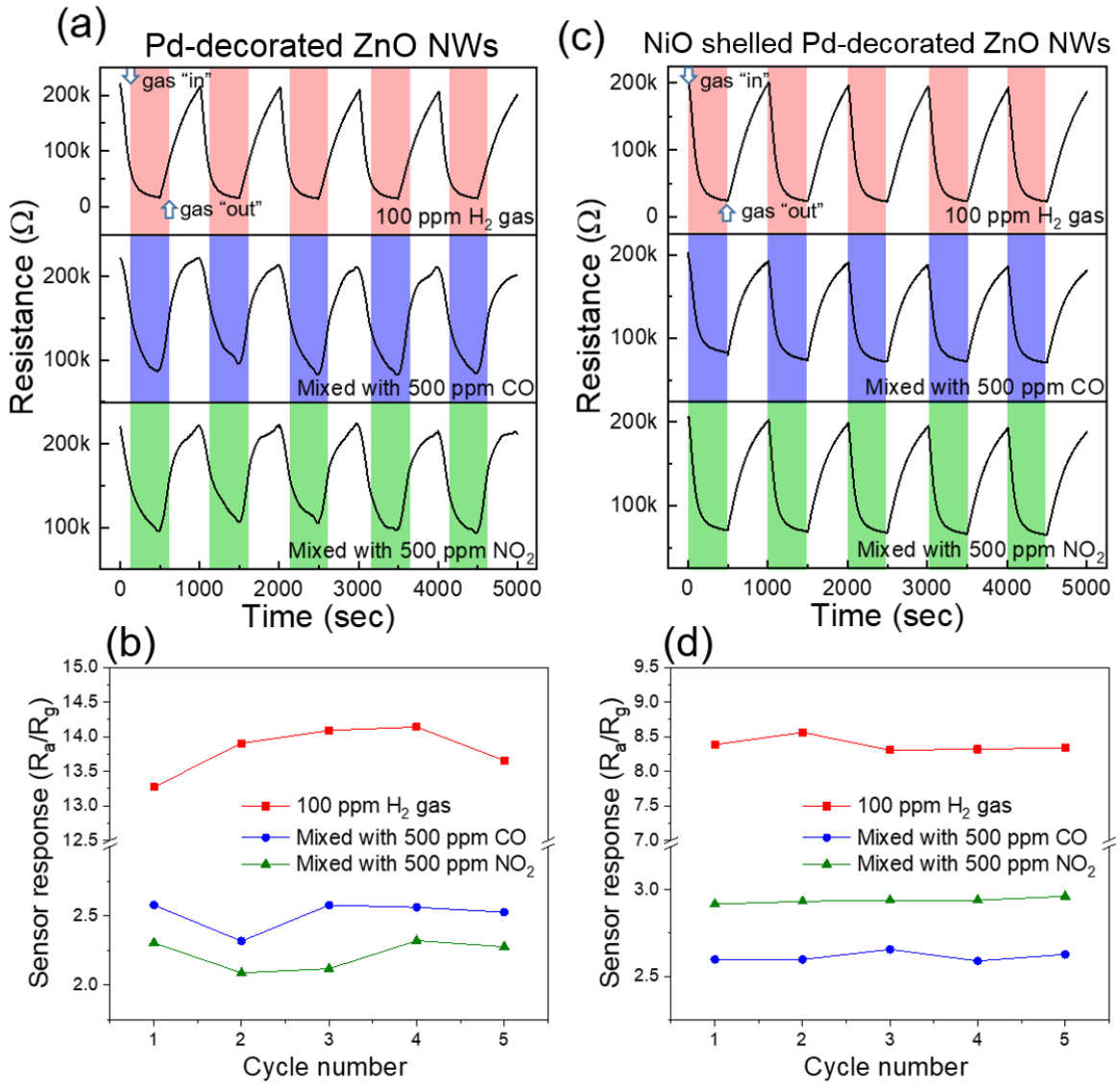

Fig. 8. Repeatability tests of (a) Pd-decorated ZnO NWs and (c) NiO-shelled Pd-decorated ZnO NWs during five sequential cycles of exposure to 100 ppm H_2 alone and to100 ppm H_2 with 500 ppm CO or 500 ppm NO_2 at 200°C. Responses in function of the cycle number of (b) Pd-decorated ZnO NWs and (d) NiO-shelled Pd-decorated ZnO NWs.

In next step, the responses of the two gas sensors to 100 ppm H_2 and 100 ppm H_2 mixed with 500 ppm CO or with 500 ppm NO_2 gas were measured in the presence of 0% and 40% relative humidity (RH) at 200°C. The dynamic resistance curves of the Pd-decorated ZnO NW gas sensor (**Fig. 9a-c**) showed that the initial resistance decreased in the presence of humidity. Indeed, the resistance of n-type semiconductors is affected by water vapors. The following reactions can take place between water molecules and adsorbed oxygen on the ZnO NWs surface, leading to the release of electrons back to the sensor surface and consequently to the decrease of the electrical resistance (Eq. 1 and 2) [40]:

$$H_2O(g) + 2Zn_{lat.} + O^-(ads) \rightarrow 2\,(Zn_{lat.} - OH) + e^- \qquad (1)$$

$$H_2O(g) + 2Zn_{lat.} + O_O \rightarrow 2\,(Zn_{lat.} - OH) + V_{\ddot{O}} + 2e^- \qquad (2)$$

Similarly, for all tested gases, the response was slightly decreased in the presence of 40% of RH (**Fig. 9d** for Pd-decorated ZnO NWs). This was explained by the fact that in a moist atmosphere, upon adsorption of water molecules at the sensor surface, the number of free sites on the sensor surface drops, thus decreasing the adsorption of target gases and consequently the sensing response.

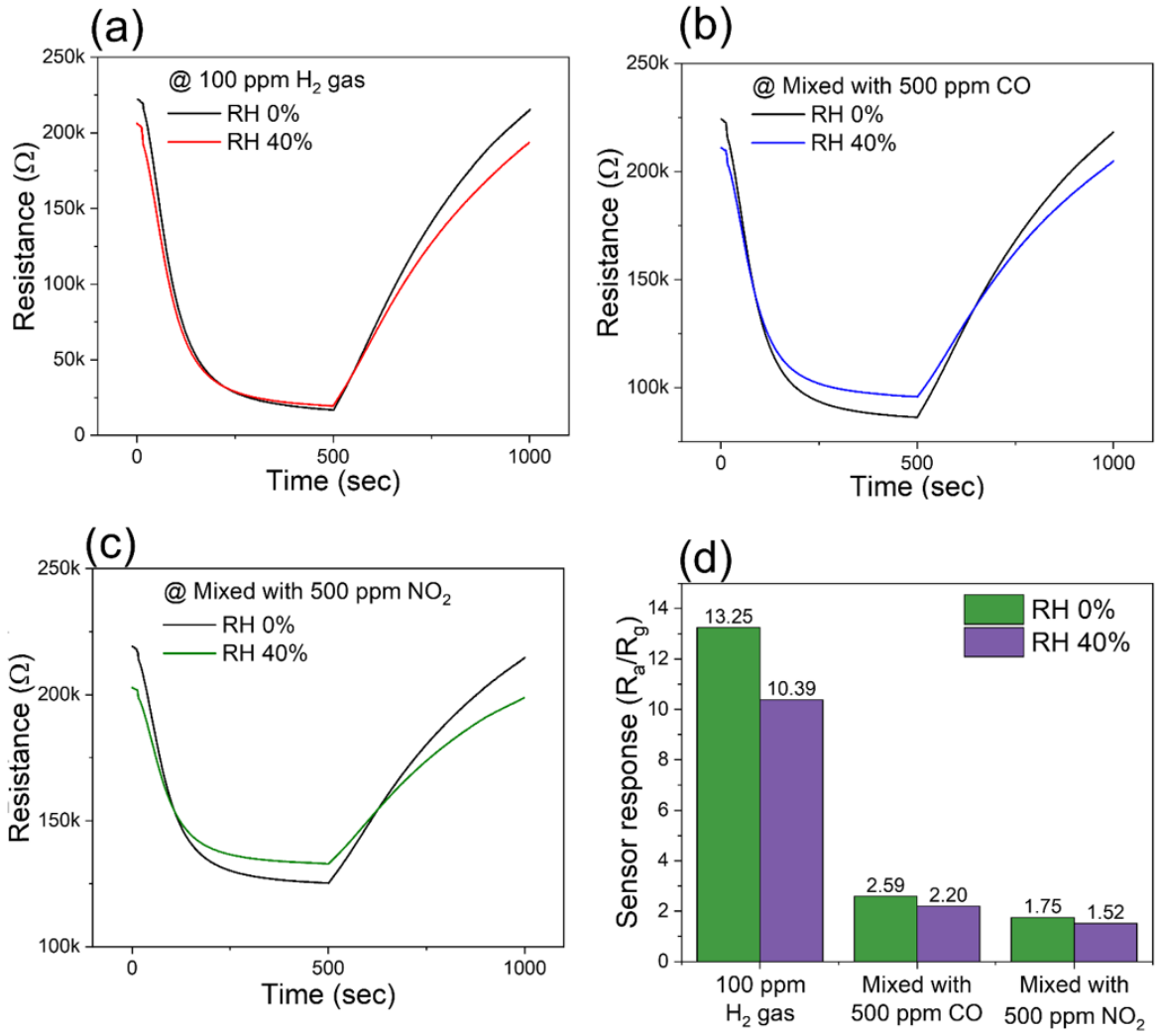

Fig. 9. Dynamic resistance of the Pd-decorated ZnO NW gas sensor in the presence of (a) 100 ppm H_2 gas, of (b) 100 ppm H_2 + 500 ppm CO, and of (c) 100 ppm H_2 + 500 ppm NO_2 in a dry (0% of RH) or moist atmosphere (40% of RH) at 200°C. (d) Comparison of Pd-decorated ZnO NW responses to the target gases in the presence of 0 and 40% of RH at 200°C.

Similarly, the initial resistance of the NiO-shelled Pd-decorated ZnO NW gas sensor decreased in the presence of 40% of RH (**Fig. 10a-c**) and the response was slightly decreased in the

presence of 40% of RH (**Fig. 10d**) for the same reasons described for the Pd-decorated ZnO NW sensor.

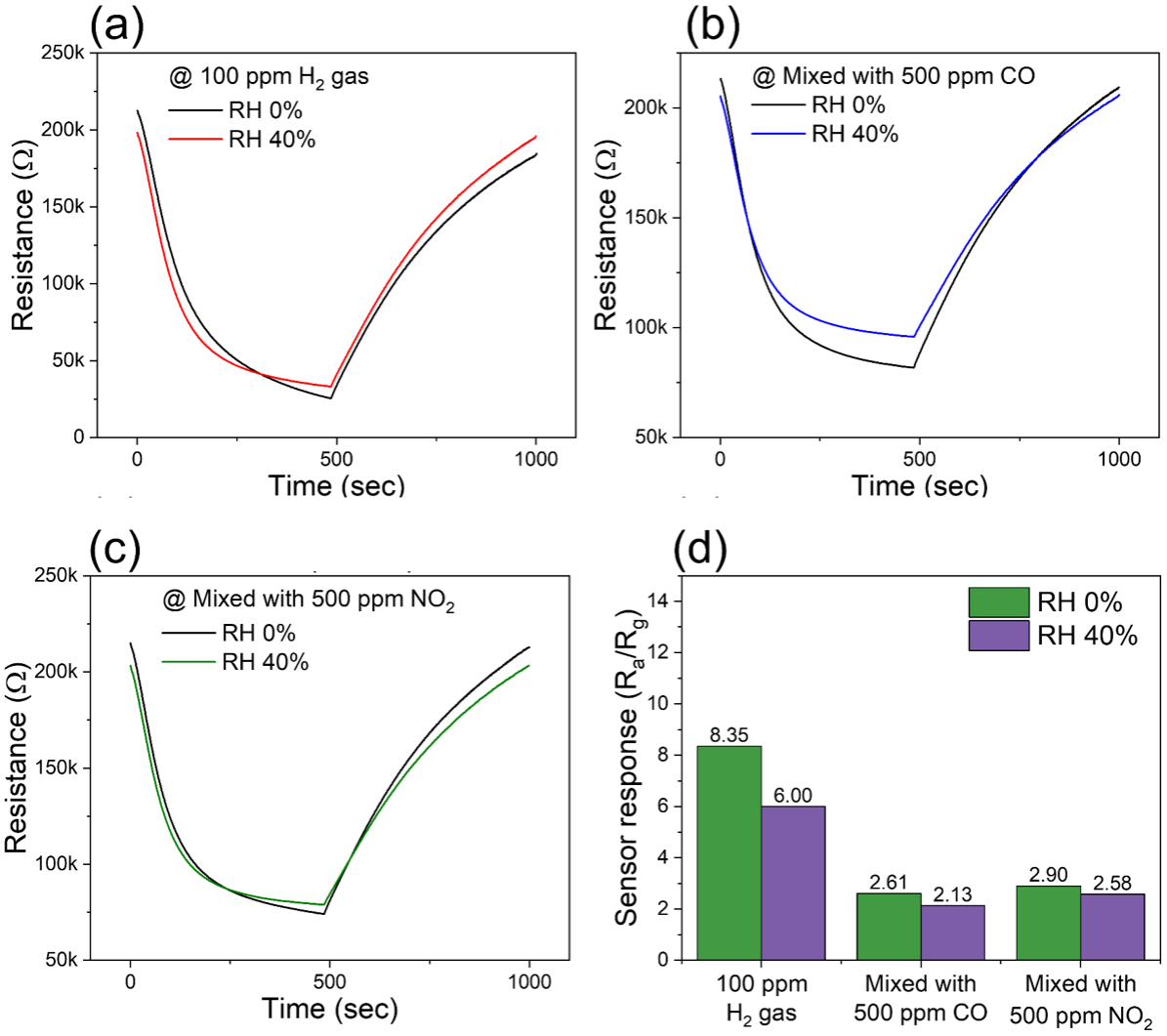

Fig. 10. Dynamic resistance of the NiO-shelled Pd-decorated ZnO NW gas sensor in the presence of (a) 100 ppm H_2, of (b) 100 ppm H_2 + 500 ppm CO, and of (c) 100 ppm H_2 + 500 ppm NO_2 in a dry (0% of RH) or moist atmosphere (40% of RH) at 200°C. (d) Comparison of the responses to the target gases in the presence of 0 and 40% of RH at 200°C.

Lastly, analysis of the response of Pd-decorated ZnO NWs (**Fig. S1a-c**) and NiO-shelled Pd-decorated ZnO NWs (**Fig. S1d-f**) to pure 100 ppm H_2 gas, 100 ppm H_2 + 500 ppm CO and 100 ppm H_2 + 500 ppm NO_2 at 200°C after 15 and 30 days showed their long-term stability. Comparison (**Fig. 11a-b**) of the responses of Pd-decorated ZnO NWs and NiO-shelled Pd-decorated ZnO NWs to target gases at 200°C just after fabrication and after 15 and 30 days showed that although the responses slightly decreased likely due to adsorption of water

molecules or of some particles from the laboratory atmosphere, they were still high even after 30 days. This good stability is important for practical applications.

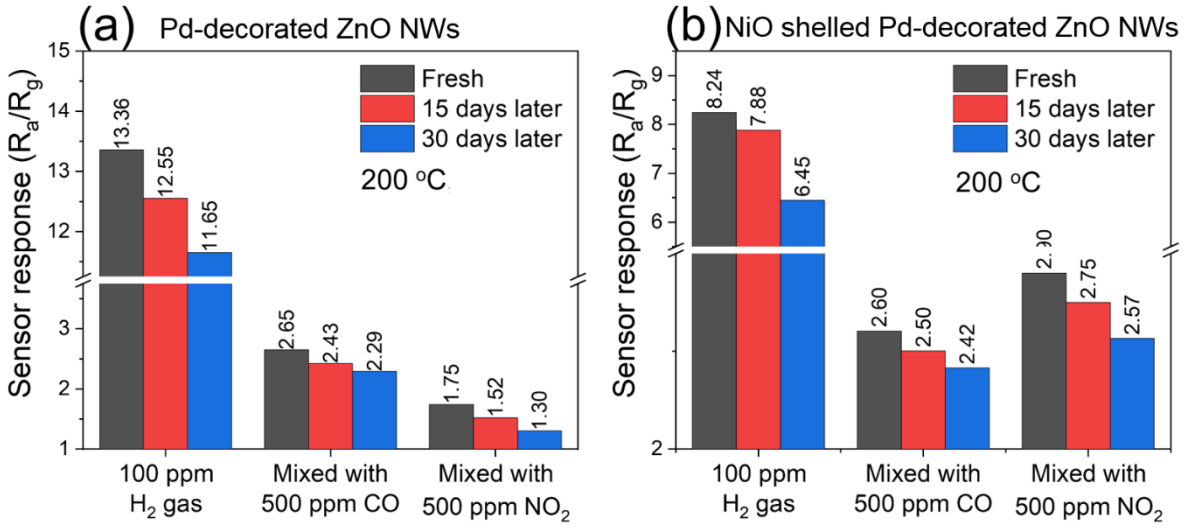

Fig. 11. Long-term stability of the response of (a) Pd-decorated ZnO NWs and (b) NiO-shelled Pd-decorated ZnO NWs to the indicated gases at 200°C just after fabrication (Fresh) and after 15 and 30 days.

3.3.2. Gas sensing mechanism

The general sensing mechanism of chemiresistive gas sensors is based on the resistance change in the presence of target gases [41]. When pristine ZnO NWs are exposed to clean air, oxygen from air will be adsorbed on their surface. Then, due to its electrophilic nature, this oxygen takes electrons from the sensor surface to which they were adsorbed as ionic species [42]:

$$O_2(g) \rightarrow O_2(ads) \quad (3)$$
$$O_2(ads) + e^- \rightarrow O_2^-(ads) \quad (4)$$
$$O_2^-(ads) + e^- \rightarrow 2O^- \quad (5)$$

The oxygen species present on the sensor surface are influenced by the surface condition and temperature. The dominant species are O_2^- and O^- for temperatures < 150°C and for 150 < temperatures < 300°C, respectively. As an electron depletion layer (EDL) is formed at the ZnO NW surface, the conductivity is confined to the ZnO NW inner sides that form a conduction channel. Due to EDL formation and the conduction channel narrowing inside ZnO NWs, the conductivity decreases relatively to the vacuum condition when oxygen is not adsorbed on the sensor surface. When added, H_2 gas is adsorbed on the ZnO NW surface where it reacts with the already adsorbed oxygen species as described in Eq. 6 [43]:

$$H_2 + O^- \rightarrow H_2O + e^- \quad (6)$$

This leads to the liberation of electrons on ZnO NW surface, followed by the EDL narrowing and the conduction channel expansion inside ZnO NWs. This contributes to the changes in the

sensor resistance and the appearance of the sensing signal. Moreover, the ZnO NW networked nature promotes the formation of homojunctions in air, in contact areas between ZnO-ZnO NWs. As a result, potential barriers are formed that hinder the electron flow from one ZnO NW to another. Upon exposure to H_2 gas, the released electrons come back to the surface, thus decreasing the height of potential barriers and contributing to the resistance modulation [12b]. Yet, the pristine ZnO NW gas sensor showed poor performance compared with other gas sensors.

To explain the improved performance of the Pd-decorated ZnO NW gas sensor, additional Pd NP-related mechanisms must be considered. Indeed, Pd is a good catalyst for splitting O_2 or H_2 molecules [44]. Pd can dissociate incoming oxygen species on its surface and the dissociated oxygen atoms can be adsorbed on the surface of neighboring ZnO in a so-called spill-over effect, leading to adsorption of more oxygen ions on the ZnO surface [45]. This increases the Pd-decorated ZnO baseline resistance compared with pristine ZnO NWs. In the presence of Pd NPs, H_2 is catalytically dissociated into H atoms that can move to neighboring ZnO surfaces (spill-over effect) [46]:

$$H_2 \xrightarrow{Pd} H + H \quad (7)$$

Then, H atoms can react freely with the previously adsorbed surface ions as follows [47]:

$$2H + O^-_{(ads)} \rightarrow H_2O + e \quad (8)$$

Hence, Pd NPs can increase the dissociation rate and the subsequent reactions of H atoms with oxygen ions, thus improving the gas sensor response.

Moreover, because of the different work function values of Pd (5.3 eV) and ZnO (4.5 eV) [45], when they are in intimate contact, electrons from ZnO move to Pd NPs to equalize the Fermi levels. Therefore, band bending occurs and Schottky barriers form between the Pd and ZnO interfaces, leading to the formation of potential barriers to the electron flow from ZnO to Pd. In addition, due to electron transfer from ZnO to Pd, EDL width on ZnO NWs increases, leading to a significant enlargement of the base resistance, as shown in **Figures 5a** and **b** for pristine and Pd-decorated ZnO NW gas sensors. Then, following exposure to H_2 gas and release of electrons back to the sensor surface, the height of the Schottky barriers changes, leading to a significant decrease of the electrical resistance. It is also possible that after H_2 dissociation on the Pd NP surface, some H atoms diffuse into the Pd lattice. Indeed, H_2 gas uptake by Pd is very high (>600 times its own volume) [12b]. Therefore, Pd can be partially converted to PdH_x ($Pd + x\ H \rightarrow PdH_x$) [48] that exhibits a lower work function and higher resistance compared with metallic Pd. Upon conversion to PdH_x in the presence of H_2 gas, the height of the initially formed Schottky barriers significantly changes, contributing to the sensor signal. Furthermore, as revealed by the XPS analysis, Pd is partially oxidized into PdO because during the deposition of the NiO shell, the oxygen source was ozone that is considered a strong oxidizing agent. Therefore, when exposed to H_2, a reducing gas, PdO should be reduced to Pd with a different resistance that contributes to the resistance change:

$$PdO + H_2 \rightarrow Pd + H_2O \quad (9)$$

All these contributions explain the higher response of the Pd-decorated ZnO sensor to H_2 gas compared with pristine ZnO NWs.

The NiO-shelled Pd-decorated ZnO NW gas sensor displayed a lower response to H_2 gas compared with Pd-decorated ZnO NWs, but a better selectivity towards H_2 gas when mixed with NO_2 and CO gases. This can be mainly attributed to fact that due to the thin continuous NiO shell deposited over the Pd-decorated ZnO NWs, Pd NPs are directly in contact with air. Therefore, PD-related sensing enhancement is limited in the NiO-shelled Pd-decorated ZnO NW gas sensor, leading to a lower response compared with Pd-decorated ZnO NWs. Furthermore, NiO response to gases is intrinsically lower than that of ZnO due to its p-type nature [49]. Therefore, after the formation of a thin NiO shell over ZnO, NiO is exposed to H_2 instead of bare ZnO.

As the NiO-shelled Pd-decorated ZnO NW gas sensor has an n-type behavior, it can be inferred that the sensing properties are still governed by ZnO (n-type semiconducting behavior) and not by p-NiO. Indeed, due to the limited thickness of the NiO shell layer, electrical transport is not fully localized on this layer, but is observed in the NiO shell and also in the ZnO core (i.e. smearing effect)[50]. Therefore, during exposure to air, the whole NiO shell is converted to a hole accumulation layer (HAL) and some ZnO NWs also are engaged in the sensing reactions. This raises the question of why the NiO-shelled Pd-decorated ZnO NWs showed a lower baseline resistance compared with the Pd-decorated ZnO NW gas sensor. In Pd-decorated ZnO NWs both adsorbed oxygen species and Pd NPs lead to extraction of electrons from ZnO, resulting in a high baseline resistance. In NiO-shelled Pd-decorated ZnO NWs, electrons move from ZnO to both Pd and NiO, leading to EDL expansion in ZnO NWs and consequently to increased resistance, as reported by Nakate et al.[19]. Moreover, some of the electrons that move from NiO to Pd are harvested by adsorbed oxygen species. These two effects cause the expansion of HAL on NiO and decrease resistance. Therefore, in NiO-shelled Pd-decorated ZnO NWs, both NiO and Pd lead to electron extraction from ZnO; however, the presence of a thin p-NiO shell, the full removal of electrons by adsorbed oxygen species and Pd NPs, and the full coverage of HAL on NiO lead to a slight reduction of resistance compared with Pd-decorated ZnO NWs gas.

In the NiO-shelled Pd-decorated ZnO NW gas sensor, three heterojunctions should be considered: NiO-ZnO, NiO-Pd Schottky, and Pd-ZnO Schottky heterojunctions. Specifically, as NiO has a work function value of 5-5.3 eV [51], at the ZnO and NiO interface, electrons move from ZnO to NiO to equalize the Fermi levels, resulting in band bending and heterojunction formation. Upon exposure to H_2 gas, the released electrons cause a reduction of the potential barrier height between ZnO and NiO, resulting in the modulation of the sensor resistance. Furthermore, as Pd work function value is higher than those of NiO and ZnO, in the areas where ZnO and NiO are in contact with Pd, electrons move from NiO and ZnO to Pd, resulting in the generation of potential barriers. Upon exposure to H_2 gas, electrons are released back to the sensor surface and the height of these potential barriers changes, contributing to the sensing signal. **Figure 12** schematically describes the energy band levels of Pd-ZnO-NiO before and after contact with air and H_2.

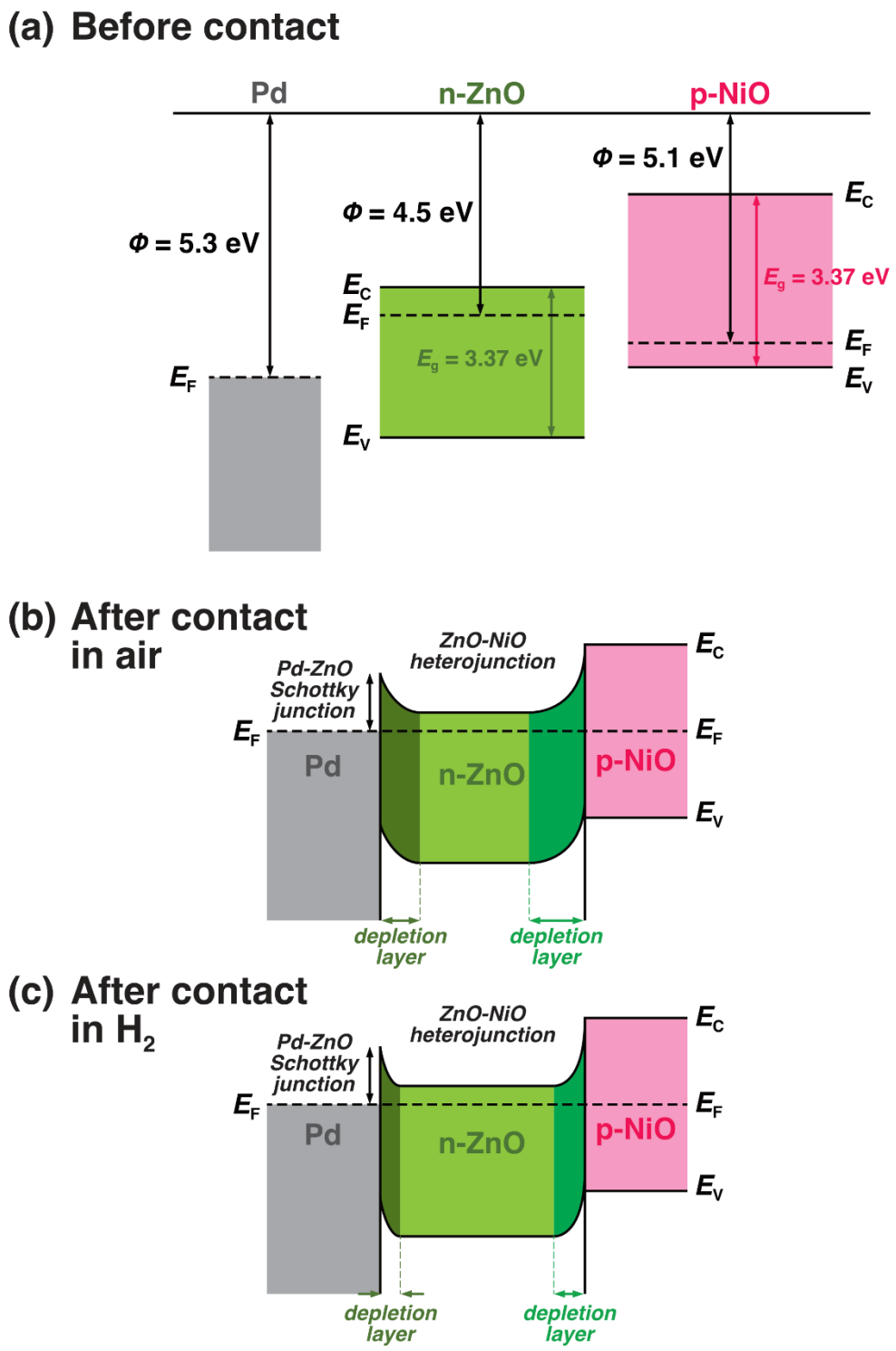

Fig. 12. Energy band levels of Pd-ZnO-NiO (a) before contact and after contact (b) in air and (c) in H_2.

Now, it is possible to explain the sensing behavior of the optimized gas sensor in the presence of mixed gases. Upon exposure to a gas mixture (H_2 and 500 ppm CO), its response decreases compared to the response to pure H_2. Like H_2, CO gas is a reducing molecule. When the sensor is exposed to CO gas, the following reaction is likely to occur [52]:

$$CO + O^- \rightarrow CO_2 + e^- \quad (9)$$

Consequently, as observed with H_2 gas, electrons move back to the sensor surface, resulting in the conductivity increase and resistance decrease. As only one electron is liberated upon reaction of CO with adsorbed oxygen species (like with H_2), the response decrease upon exposure to CO gas is not linked to electron-donating effects. The response decrease in the presence of CO can be related to (i) the sensing temperature and (ii) the larger size of CO molecules relative to H_2. Indeed, as each gas has its own unique characteristics, depending on the surface condition and gas type, the maximum adsorption of a gas at the sensor surface occurs at a specific temperature, which may differ for different gases. Our results suggest that 200°C is not the optimal sensing temperature for CO gas. Moreover, CO molecules have a larger kinetic diameter (3.70Å) [53] than H_2 molecules (2.89Å) [54]. Assuming the same adsorption sites on the sensor surface, CO molecules can occupy more adsorption sites due to their larger size when they are mixed with H_2 gas. This leads to a reduction of sites for H_2 gas adsorption and consequently to a lower gas sensor response in the presence of gas mixtures containing H_2 + CO.

Concerning the slight decrease of the response in the presence of H_2 + NO_2 gas mixtures, NO_2 can react with oxygen species adsorbed to the sensor surface or directly collect electrons from the sensor surface, leading to the following reactions [55]:

$$NO_2(g) \rightarrow NO_2(ads)$$

$$NO_2(g) + e^- \rightarrow NO_2^-(ads) \quad (10)$$

$$NO_2(g) + 2O^- + e^- \rightarrow NO_2\,(g) + 2O^{2-} \quad (11)$$

According to these reactions, the collection of electrons by adsorbed NO_2 results in a resistance increase. However, in the presence of H_2 + NO_2 gas mixtures, the overall resistance decreased, reflecting the fact that the gas sensor is more sensitive to H_2 than to NO_2. As previously discussed, the reduced response to such mixture can be partly explained by the larger size of NO_2, compared with H_2, and the sensing temperature.

4. Conclusions

Pristine ZnO NW, Pd-decorated ZnO NW and NiO shelled Pd-decorated ZnO NW gas sensors were fabricated for H_2 sensing studies. Using ALD, Pd NPs and a NiO shell were coated over the as-grown ZnO NWs. The morphology, crystalline nature, phase and chemical composition studies demonstrated the synthesis of materials with the expected features. The gas sensing studies showed the pristine ZnO NWs gas sensor poor performance towards H_2 gas compared with the other two gas sensors. At 200°C, the responses of the Pd-decorated ZnO NW and NiO-shelled Pd-decorated ZnO NW gas sensors to 500 ppm H_2 gas were 41.01 and 16.12. When gas mixtures were used, the NiO-shelled Pd-decorated ZnO NW gas sensor demonstrated superior selectivity to H_2 compared with the Pd-decorated ZnO NW sensor: 13.19 versus 6.39 to 500 ppm H_2 + 500 ppm NO_2 and 12.41 versus 12.11 to 500 ppm H_2 + 500 ppm CO, respectively. These results highlight the enhanced selectivity of the NiO-shelled Pd-decorated ZnO NW gas sensor to H_2 gas in the presence of H_2 + CO and H_2 + NO_2 gas mixtures. The enhanced performance of the optimized sensor was related to the formation of NiO-ZnO

heterojunctions, NiO-Pd Schottky junctions and Pd-ZnO Schottky junctions, the catalytic effect of Pd and the nature of H_2 gas (small kinetic diameter). This study demonstrated that it is possible to develop a highly selective H_2 gas sensor in realistic conditions.

Acknowledgements

The authors acknowledge D. Chaudanson and A. Altié (CINaM) for their valuable help with electron microscopy. Aurélien Renard (University of Lorraine, Nancy, France) is acknowledged for XPS measurements. This collaborative work was supported by the French Agence Nationale de la Recherche (ANR) under grant ANR-17-CE09-0049-03 (project MENINA). Sang Sub Kim acknowledges the support from the Korea Polar Research Institute (KOPRI) grant funded by the Ministry of Oceans and Fisheries (KOPRI project No. PE22900), and a National Research Foundation of Korea (NRF) grant funded by the Korean government (MSIT) [No. 2021R1A2C1009790].

References

[1] a) X. Meng, M. Bi, Q. Xiao, W. Gao, *Sens. Actuators, B* **2022**, 359; b) H.-D. Dong, J.-P. Zhao, M.-X. Peng, Y.-H. Zhang, P.-Y. Xu, *Vacuum* **2023**, 207; c) S. Lu, Y. Zhang, J. Liu, H.-Y. Li, Z. Hu, X. Luo, N. Gao, B. Zhang, J. Jiang, A. Zhong, J. Luo, H. Liu, *Sens. Actuators, B* **2021**, 345; d) A. Mirzaei, H. R. Yousefi, F. Falsafi, M. Bonyani, J.-H. Lee, J.-H. Kim, H. W. Kim, S. S. Kim, *Int. J. Hydrogen Energy* **2019**, 44, 20552; e) H. Bai, H. Guo, Y. Tan, J. Wang, Y. Dong, B. Liu, Z. Xie, F. Guo, D. Chen, R. Zhang, Y. Zheng, *Sens. Actuators, B* **2021**, 340.

[2] R. Yonamine, Y. Satoh, M. Kodama, Y. Araki, T. Kazama, *Anesthesiology* **2013**, 118, 105.

[3] a) G. Korotcenkov, B. K. Cho, *Sens. Actuators, B* **2013**, 188, 709; b) A. Mirzaei, S. G. Leonardi, G. Neri, *Ceram. Int.* **2016**, 42, 15119; c) A. Mirzaei, G. Neri, *Sens. Actuators, B* **2016**, 237, 749.

[4] H.-J. Kim, J.-H. Lee, *Sens. Actuators, B* **2014**, 192, 607.

[5] L. Zhu, W. Zeng, *Sens. Actuators, A* **2017**, 267, 242.

[6] C. N. Wang, Y. L. Li, F. L. Gong, Y. H. Zhang, S. M. Fang, H. L. Zhang, *Chem Rec* **2020**, 20, 1553.

[7] M. Kamal Hossain, Q. Ahmed Drmosh, *Chem Rec* **2022**, 22.

[8] M. A. Franco, P. P. Conti, R. S. Andre, D. S. Correa, *Sens Actuators Rep* **2022**, 4.

[9] A. Singh, S. Sikarwar, A. Verma, B. Chandra Yadav, *Sens. Actuators, A* **2021**, 332.

[10] J. van den Broek, I. C. Weber, A. T. Guntner, S. E. Pratsinis, *Mater Horiz* **2021**, 8, 661.

[11] a) S. Mourya, A. Kumar, J. Jaiswal, G. Malik, B. Kumar, R. Chandra, *Sens. Actuators, B* **2019**, 283, 373; b) A. Kumar, Y. Zhao, M. M. Mohammadi, J. Liu, T. Thundat, M. T. Swihart, *ACS Sens* **2022**, 7, 225.

[12] a) Y. Wang, X. Meng, M. Yao, G. Sun, Z. Zhang, *Ceram. Int.* **2019**, 45, 13150; b) J. H. Lee, J. H. Kim, J. Y. Kim, A. Mirzaei, H. W. Kim, S. S. Kim, *Sensors* **2019**, 19.

[13] K. Hu, F. Wang, Z. Shen, H. Liu, J. Xiong, *J. Alloys Compd* **2021**, 850.

[14] M. Honkanen, J. Wang, M. Kärkkäinen, M. Huuhtanen, H. Jiang, K. Kallinen, R. L. Keiski, J. Akola, M. Vippola, *J. Catal.* **2018**, 358, 253.

[15] P. Rai, S. M. Majhi, Y.-T. Yu, J.-H. Lee, *RSC Adv.* **2015**, 5, 76229.

[16] J. H. Lee, J. Y. Kim, A. Mirzaei, H. W. Kim, S. S. Kim, *Nanomaterials* **2018**, 8.

[17] a) N. D. Hoa, P. Van Tong, C. M. Hung, N. Van Duy, N. Van Hieu, *Int. J. Hydrogen Energy* **2018**, 43, 9446; b) N. Jayababu, M. Poloju, J. Shruthi, M. V. R. Reddy, *Mater. Sci. Semicond. Process.* **2019**, 102; c) Y.-C. Liang, Y.-C. Chang, *CrystEngComm* **2020**, 22, 2315; d) Y. Sun, Z. Zhao, K. Suematsu, P. Li, W. Zhang, J. Hu, *Mater. Res. Bull.* **2022**, 146; e) A. Singh, B. C. Yadav, *Results Surf. Interfaces* **2023**, 11.

[18] a) D. Li, Y. Zhang, D. Liu, S. Yao, F. Liu, B. Wang, P. Sun, Y. Gao, X. Chuai, G. Lu, *CrystEngComm* **2016**, 18, 8101; b) L. Xu, R. Zheng, S. Liu, J. Song, J. Chen, B. Dong, H. Song, *Inorg Chem* **2012**, 51, 7733.

[19] U. T. Nakate, R. Ahmad, P. Patil, Y. Wang, K. S. Bhat, T. Mahmoudi, Y. T. Yu, E.-k. Suh, Y.-B. Hahn, *J. Alloys Compd.* **2019**, 797, 456.

[20] V. Cremers, R. L. Puurunen, J. Dendooven, *Appl. Phys. Rev.* **2019**, 6, 021302.

[21] a) M. Weber, C. Lamboux, B. Navarra, P. Miele, S. Zanna, M. E. Dufond, L. Santinacci, M. Bechelany, *Nanomaterials* **2018**, 8; b) C. Badie, J.-H. Lee, A. Mirzaei, H. W. Kim, S. Sayegh, M. Bechelany, L. Santinacci, S. S. Kim, *J. Mater. Chem. A* **2023**, 11, 12202.

[22] a) J. W. Elam, A. Zinovev, C. Y. Han, H. H. Wang, U. Welp, J. N. Hryn, M. J. Pellin, *Thin Solid Films* **2006**, 515, 1664; b) M. Lindblad, L. P. Lindfors, T. Suntola, *Catal. Lett.* **1994**, 27, 323; c) H. L. Lu, G. Scarel, C. Wiemer, M. Perego, S. Spiga, M. Fanciulli, G. Pavia, *J. Electrochem. Soc.* **2008**, 155.

[23] L. Assaud, E. Monyoncho, K. Pitzschel, A. Allagui, M. Petit, M. Hanbücken, E. A. Baranova, L. Santinacci, *Beilstein J. Nanotechnol.* **2014**, 5, 162.

[24] A. Barhoum, H. H. El-Maghrabi, I. Iatsunskyi, E. Coy, A. Renard, C. Salameh, M. Weber, S. Sayegh, A. A. Nada, S. Roualdes, M. Bechelany, *J Colloid Interface Sci* **2020**, 569, 286.

[25] J. Xie, X. Liu, S. Jing, C. Pang, Q. Liu, J. Zhang, *ACS Appl Mater Interfaces* **2021**, 13, 39621.

[26] J.-H. Kim, A. Mirzaei, H. W. Kim, S. S. Kim, *Sens. Actuators, B* **2019**, 297.

[27] a) J.-H. Kim, J.-H. Lee, Y. Park, J.-Y. Kim, A. Mirzaei, H. W. Kim, S. S. Kim, *Sens. Actuators, B* **2019**, 294, 78; b) J. H. Kim, A. Mirzaei, H. W. Kim, S. S. Kim, *ACS Appl Mater Interfaces* **2019**, 11, 24172.

[28] C. H. Ahn, S. G. Cho, H. J. Lee, K. H. Park, S. H. Jeong, *Met. Mater. Int.* **2001**, 7, 621.

[29] M. Weber, P. Collot, H. El Gaddari, S. Tingry, M. Bechelany, Y. Holade, *ChemElectroChem* **2018**, 5, 743.

[30] M. K. S. Barr, L. Assaud, Y. Wu, C. Laffon, P. Parent, J. Bachmann, L. Santinacci, *Electrochim. Acta* **2015**, 179, 504.

[31] a) T. L. H. Doan, J.-Y. Kim, J.-H. Lee, L. H. T. Nguyen, Y. T. Dang, K.-B. T. Bui, A. T. T. Pham, A. Mirzaei, T. B. Phan, S. S. Kim, *Sens. Actuators, B* **2021**, 348; b) T. L. H. Doan, J.-Y. Kim, J.-H. Lee, L. H. T. Nguyen, H. T. T. Nguyen, A. T. T. Pham, T. B. Nguyen Le, A. Mirzaei, T. B. Phan, S. S. Kim, *Sens. Actuators, B* **2021**, 349.

[32] a) D. Wagner, W. M. Riggs, L. E. Davis, J. F. Moulder, *Handbook of X-ray Photoelectron Spectroscopy*, Perkin-Elmer Corp., Physical Electronics Division, Eden Prairie, Minnesota, USA **1979**; b) M. Weber, J. Y. Kim, J. H. Lee, J. H. Kim, I. Iatsunskyi, E. Coy, P. Miele, M. Bechelany, S. S. Kim, *J. Mater. Chem. A* **2019**, 7, 8107.

[33] a) M. A. Peck, M. A. Langell, *Chem. Mater.* **2012**, 24, 4483; b) R. Islam, G. Chen, P. Ramesh, J. Suh, N. Fuchigami, D. Lee, K. A. Littau, K. Weiner, R. T. Collins, K. C. Saraswat, *ACS Appl Mater Interfaces* **2017**, 9, 17201.

[34] L. Assaud, N. Brazeau, M. K. S. Barr, M. Hanbücken, S. Ntais, E. A. Baranova, L. Santinacci, *ACS Appl. Mater. Interfaces* **2015**, 7, 24533.

[35] M. K. S. Barr, L. Assaud, N. Brazeau, M. Hanbücken, S. Ntais, L. Santinacci, E. A. Baranova, *J. Phys. Chem. C* **2017**, 121, 17727.

[36] J. Dabboussi, R. Abdallah, L. Santinacci, S. Zanna, A. Vacher, V. Dorcet, S. Fryars, D. Floner, G. Loget, *J. Mater. Chem. A* **2022**, 10, 19769.

[37] T. Chen, S.-Y. Liu, Q. Xie, C. Detavernier, R. L. Meirhaeghe, X.-P. Qu, *Appl. Phys. A* **2009**, 98, 357.

[38] L. Santinacci, M. Bouttemy, M. Petit, A.-M. Gonçalves, N. Simon, J. Vigneron, A. Etcheberry, *J. Electrochem. Soc.* **2018**, 165, H3131.

[39] J. F. Moulder, J. Chastain, *Handbook of X-ray Photoelectron Spectroscopy: A Reference Book of Standard Spectra for Identification and Interpretation of XPS Data*, Physical Electronics Division, Perkin-Elmer Corporation, **1992**.

[40] J. W. Yoon, J. H. Lee, *Lab Chip* **2017**, 17, 3537.

[41] H. R. Ansari, A. Mirzaei, H. Shokrollahi, R. Kumar, J.-Y. Kim, H. W. Kim, M. Kumar, S. S. Kim, *J. Mater. Chem. C* **2023**, 11, 6528.

[42] a) T.-Y. Chang, A. Kumar Singh, J.-H. Shao, C.-Y. Huang, J.-M. Shieh, D.-S. Wuu, P.-L. Liu, R.-H. Horng, *Appl. Surf. Sci.* **2023**, 637; b) S. Mobtakeri, S. Habashyani, Ö. Çoban, H. F. Budak, A. E. Kasapoğlu, E. Gür, *Sens. Actuators, B* **2023**, 381.

[43] M. Moschogiannaki, L. Zouridi, J. Sukunta, S. Phanichphant, E. Gagaoudakis, C. Liewhiran, G. Kiriakidis, V. Binas, *Sens. Actuators, B* **2020**, 324.

[44] M. S. Barbosa, P. H. Suman, J. J. Kim, H. L. Tuller, J. A. Varela, M. O. Orlandi, *Sens. Actuators, B* **2017**, 239, 253.

[45] H. Kim, Y. Pak, Y. Jeong, W. Kim, J. Kim, G. Y. Jung, *Sens. Actuators, B* **2018**, 262, 460.

[46] S. M. Iordache, E. I. Ionete, A. M. Iordache, E. Tanasa, I. Stamatin, C. E. Ana Grigorescu, *Int. J. Hydrogen Energy* **2021**, 46, 11015.

[47] K. Karuppasamy, A. Sharma, D. Vikraman, Y. A. Lee, P. Sivakumar, J. G. Korvink, H. S. Kim, B. Sharma, *J. Colloid Interface Sci.* **2023**, DOI: 10.1016/j.jcis.2023.07.046.

[48] a) W. Wang, X. Liu, S. Mei, Y. Jia, M. Liu, X. Xue, D. Yang, *Sens. Actuators, B* **2019**, 287, 157; b) H.-J. Le, D. Van Dao, Y.-T. Yu, *J. Mater. Chem. A* **2020**, 8, 12968.

[49] M. Hübner, C. E. Simion, A. Tomescu-Stănoiu, S. Pokhrel, N. Bârsan, U. Weimar, *Sens. Actuators, B* **2011**, 153, 347.

[50] S. W. Choi, A. Katoch, G. J. Sun, J. H. Kim, S. H. Kim, S. S. Kim, *ACS Appl Mater Interfaces* **2014**, 6, 8281.

[51] a) P. Rai, J. W. Yoon, H. M. Jeong, S. J. Hwang, C. H. Kwak, J. H. Lee, *Nanoscale* **2014**, 6, 8292; b) H.-L. Yip, A. K. Y. Jen, *Energy Environ. Sci* **2012**, 5.

[52] J.-H. Kim, I. Sakaguchi, S. Hishita, T. Ohsawa, T. T. Suzuki, N. Saito, *Sens. Actuators, B* **2023**, 382.

[53] R. M. Prasad, A. Gurlo, R. Riedel, M. Hübner, N. Barsan, U. Weimar, *Sens. Actuators, B* **2010**, 149, 105.

[54] W.-H. Lin, T.-S. Chung, *J. Memb. Sci.* **2001**, 186, 183.

[55] H. Fang, E. Shang, D. Wang, X. Ma, B. Zhao, C. Han, C. Zheng, *Sens. Actuators, B* **2023**, 393.